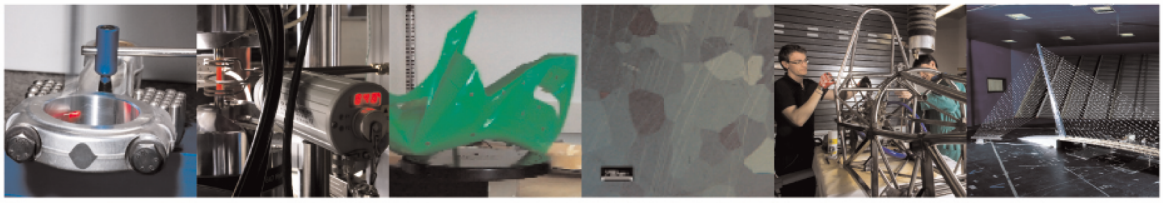
POLITECNICO
MILANO 1863

DIPARTIMENTO DI MECCANICA

mecc



AGREE: A Compliant-Controlled Upper-Limb Exoskeleton for Physical Rehabilitation of Neurological Patients

Dalla Gasperina, Stefano;Gandolla, Marta;Longatelli, Valeria;Panzenbeck, Mattia;Luciani, Beatrice;Braghin, Francesco;Pedrocchi, Alessandra

This is a post-peer-review, pre-copyedit version of S. Dalla Gasperina et al., "AGREE: A Compliant-Controlled Upper-Limb Exoskeleton for Physical Rehabilitation of Neurological Patients," in IEEE Transactions on Medical Robotics and Bionics, vol. 5, no. 1, pp. 143-154, Feb. 2023, doi: 10.1109/TMRB.2023.3239888

© 2023 IEEE. Personal use of this material is permitted. Permission from IEEE must be obtained for all other uses, in any current or future media, including reprinting/republishing this material for advertising or promotional purposes, creating new collective works, for resale or redistribution to servers or lists, or reuse of any copyrighted component of this work in other works.

This content is provided under CC BY-NC-ND 4.0 license

DIPARTIMENTO DI MECCANICA ■ POLITECNICO DI MILANO
via G. La Masa, 1 ■ 20156 Milano ■ EMAIL (PEC): pecmecc@cert.polimi.it
http://www.mecc.polimi.it
Rev. 0

AGREE: A compliant-controlled upper-limb exoskeleton for physical rehabilitation of neurological patients

Stefano Dalla Gasperina[1,3], Marta Gandolla[2,3], Valeria Longatelli[1,3], Mattia Panzenbeck[2,3], Beatrice Luciani[1,3], Francesco Braghin[2,3] and Alessandra Pedrocchi[1,3]

***Abstract*— In this work, we introduce the AGREE exoskeleton, a robotic device designed to assist in upper-limb physical rehabilitation for post-stroke survivors. We detail the exoskeleton design at the mechatronic, actuation, and control levels. The AGREE exoskeleton features a lightweight and adaptable mechanical design, which can be used with both the right and left arm, supporting three active degrees-of-freedom at the shoulder and one at the elbow. The device embodies a spring-pulley anti-gravity system to minimize torque requirements and has torque sensors on each joint for safe and smooth interaction with the user. The AGREE control system, which employs a loadcell-based impedance control method, offers various modes of human-robot interaction, such as passive-assisted, active-assisted and active-resistive exercises. Results from our experimental characterization demonstrate that the exoskeleton is capable of both compliant and rigid behavior, providing a wide range of haptic impedance and transparent behavior to both user-generated and therapist-generated forces. Our findings indicate that the AGREE exoskeleton may be a viable option for safely assisting patients with neurological conditions.**

***Index Terms*— Upper-limb exoskeleton, robotic rehabilitation, compliant control, physical human-robot interaction (pHRI).**

I. INTRODUCTION

Worldwide, a significant portion of people suffers from chronic physical impairment caused by neurological injuries and diseases [1]. Stroke, in particular, is one of the leading causes of death and permanent disability [2], and a major economic load in terms of both healthcare costs and societal informal care resources [3].

Hence, regaining lost functionalities is a primary goal for post-stroke survivors in the early sub-acute phase, and rehabilitation treatment is mandatory for effective motor recovery after neurological injuries [1]. Rehabilitation robots can support therapists and supplement therapist-like training, allowing participants to perform high-dose, high-intensity repetitive movements [4]. The literature suggests maximizing participants' engagement during the rehabilitation session and training them with personalized and challenging functional tasks [5], [6]. In this view, despite their high complexity, upper-limb exoskeletons are gaining increasing interest in research and clinical applications, as they provide therapists with a versatile tool to deliver personalized rehabilitation treatment.

The goal of rehabilitation exoskeletons is to promote the recovery process of neurological patients by supporting motor functions through soft and gentle interaction. Numerous upper-limb exoskeletons have been developed in the past decades [7]. Most of them actuate all the shoulder joints, including the scapulohumeral rhythm, such as [8] or [9]. While these approaches reduce undesired interaction forces at the shoulder girdle, they result in expensive solutions that introduce additional degrees-of-freedom at the shoulder. Other approaches employ passive mechanisms for joint self-alignment [10] or approximate the shoulder girdle to a ball-socket joint [11].

Despite the growing field of robot-assisted rehabilitation, one open question regards the development of cooperative, personalized, and adaptable control solutions to follow the patient's progress through a variety of training modalities. To tackle these needs, exoskeletons should render a broad range of haptic impedance, promoting both rigid and compliant behavior.

In detail, to make exoskeletons compliant with human motion, several hardware and control solutions have been proposed [12]. For instance, most rehabilitation robots rely on the intrinsic backdrivability of the actuation units, which can be improved through model-based friction and inertia compensation models [13], [9]. In other works, robot transparency is obtained through appropriate force/torque sensing to minimize the interaction forces at the interface points [14], [15]. Alternatively, compliant shared interaction can be obtained through series elastic actuators, which reduce the intrinsic mechanical stiffness of the electric gear-motors to promote safe and compliant interaction [8], [10], [16]. Also, series elastic actuators are well suited to indirectly measure the interaction effort between the human and the robot, but they usually introduce more complex control issues for robust control [17].

Within this context, this paper presents a novel mechatronic upper-limb exoskeleton designed for post-stroke neurorehabilitation, called AGREE exoskeleton. In this work, we strive to focus on the essential features for clinical applicability, aiming at a simple yet functional mechatronic and control design. In particular, we combined some mechatronic features that have already been presented in other exoskeletons, such as having a re-configurable arm that can

*This work was conducted thanks to the AGREE project, and it was supported by Regione Lombardia, Italy, under the ERDF ROP 2014-2020. Identifier: ARCA_2018_132

[1]NearLab, Department of Electronics, Information and Bioengineering, Politecnico di Milano, Italy. SDG is the corresponding author stefano.dallagasperina@polimi.it

[2]Department of Mechanical Engineering, Politecnico di Milano, Italy.

[3]WE-COBOT laboratory, Polo Territoriale di Lecco, Politecnico di Milano, Lecco, Italy.

SDG, MG, FB, and AP hold shares in AGADE srl, Milan, Italy.

be worn alternatively on the right or left arm [18], and having a spring-pulleys anti-gravity system (AGS) embedded into the shoulder flexion/extension actuator.

The major contribution of this work regards the use of torsional loadcells at the joints, as compared to SEAs or force/torque sensors at the interface points, for direct measurement of the interaction torques between the robotic system and the arm. We developed a layered control architecture based on an impedance control method that was previously tested on a single-joint orthosis [19]. In our previous work, we demonstrated that the developed control system could achieve a wide range of haptic impedance and promote *human-passive* and *human-active* human-robot interaction. In this work, we replicated the approach at each joint of the exoskeleton and characterized the performance of the control system on the multi-joint rehabilitation platform. This feature allows the exoskeleton to behave smoothly and compliantly against both user-generated and externally-applied forces [19].

The rest of the paper is organized as follows. Section II describes the AGREE mechatronic design. The control system is reported in Sec. III and Sec. IV presents the experimental results of the system characterization, which are discussed in Sec. V. Finally, Sec. VI draws the conclusions of the work.

II. EXOSKELETON DESIGN

A. Mechatronic design

AGREE is a powered exoskeleton intended to assist neurological patients during seated rehabilitative exercises [20] (i.e., hand-to-mouth, lateral elevation, and arm reaching exercises), and we strove to develop a mechanical design that i) permits the use of the system (with the same range of motion) on both the right and left arm, ii) is lightweight for easier portability, iii) generates joint torques to compensate the arm weight of the 95^{th} percentile male [21], and iv) assists joint movements up to 2 rad/s [22]. The exoskeleton consists of a four degrees-of-freedom (DOF) open serial chain of aluminum and steel links embodied with custom-shaped parts and cable-driven mechanisms to transmit forces from the actuation units to the interface contact points, located at the upper arm and forearm. The designed active ranges-of-motion (ROMs) of the exoskeleton, shown in Tab. I, were based on a selection of activities of daily living that can be carried out at the table [23]. The first three joints are intended to replicate the movements of the ball-socket joint of the shoulder complex, which is implemented through a series of three coincident and mutually orthogonal rotational axes. To simplify our design and reduce production costs, the shoulder center of rotation is supposed to be fixed, which is considered an acceptable approximation for the required ROM [11], although the shoulder center of rotation is known to vary with arm humeral elevation [24]. The fourth joint is aligned with the elbow flexion/extension anatomical joint. The exoskeleton is secured to the user through arm cuffs at the upper arm and forearm that are provided in different sizes to accommodate different arms, and are internally covered with washable, breathable, and an-allergic tissue.

The AGREE exoskeleton mechanical structure is composed of four modular active joints. Each module is embodied with its own actuation unit and transmission mechanism, as shown in Fig. 1. The actuation unit architecture is presented in Sec. II-B.

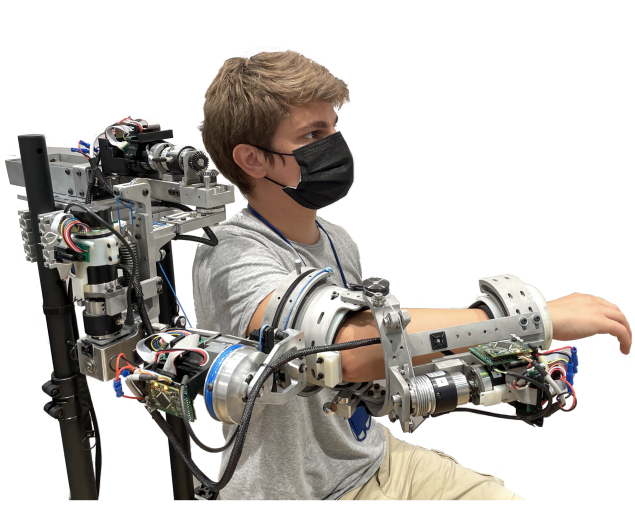
The first module, J_1 unit, drives the shoulder horizontal abdo/adduction (S-AA). To optimize encumbrance and mass distribution, the motor axis M_1 (blue axis) is placed horizontally in the rear part of the system and connects through a conical bevel gear to actuate the vertical joint axis J_1 (red axis).

Similarly, the J_2 module has a vertical motor axis M_2, and a bevel gear transmits the motion to the horizontal shoulder flexion/extension axis (S-FE). Following the "azimuth-elevation-roll" convention [25], the rotational axis of the second joint, namely "elevation", is always parallel to ground and, as such, it always experiences the highest gravitational torque demands in the kinematic chain. For this reason, we provided the J_2 module with a passive spring-based anti-gravity system (AGS) that generates an additional gravity compensation force. The advantages provided by the AGS are twofold. Firstly, it provides an always-positive torque offset that counterbalances arm lifting movements. Indeed, the AGS was integrated on the joint that experiences the highest torque demand in the kinematic chain to reduce the motor torque requirements during arm lifting tasks. Secondly, the AGS brings the benefit that the robot does not abruptly collapse in case of power loss, improving the mechanical safety of the system [18].

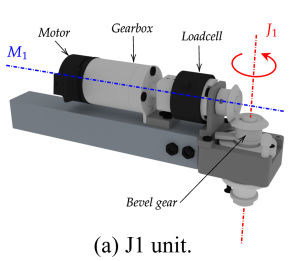
The actuation of the shoulder rotation around the humeral axis, i.e., shoulder or humeral rotation (S-HR), has been deeply studied in the literature. In fact, the humeral rotation movement does not permit the traditional serial joint configuration, but it needs to employ rotating cuffs/shells [11], [18] or complex shoulder mechanisms [8], [9], [15]. In our design, we positioned the J_3 module along the user's arm (Fig. 1), as in [18], [16]. The actuation chain comprises a semi-cylindrical aluminum shell that rotates around its central axis through a cable-driven capstan mechanism. A bowl-shaped capstan pulley, wrapped by a Dyneema® cable, is anchored to the shell's extremities, and forces the shell to slide along a custom-made curved rail, constituted of several pins sliding inside a curvilinear guide. The capstan-drive introduces an additional transmission reduction of 3:1, as shown in Tab. I. As a result, the motor axis M_3 is always parallel to the joint axis J_3, and the actuation mechanism covers the outer side of the arm, facilitating donning and doffing procedures, also for hypertonic, spastic, or severely impaired participants.

The J_4 module operates the elbow flexion/extension (E-FE). In this case, the 90° rotation between M_4 and J_4 axes is introduced to reduce the encumbrance around the elbow area, and we placed the J_4 unit along the forearm, so as that the motor axis M_4 is parallel to the forearm. Then, a capstan drive transmits the motion to the elbow joint axis J_4 through a Dyneema® cable and two fixed pulleys. A string tensioner can be used to set the cable pre-tension.

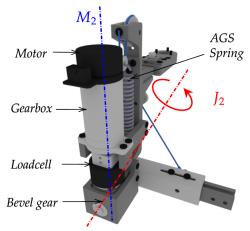
Lastly, a passive joint is added to permit wrist prona-



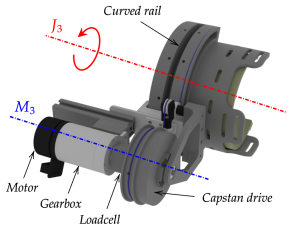
(a) The right-sided AGREE exoskeleton.



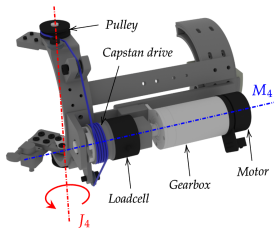
(a) J1 unit.



(b) J2 unit.



(c) J3 unit.



(d) J4 unit.

Fig. 1: The AGREE exoskeleton has a modular structure. The actuation unit is replicated for each joint, eventually coupled through a transmission mechanism. (a) J_1: shoulder horizontal adduction/abduction, (b) J_2: shoulder flexion/extension, (c) J_3: shoulder humeral intra/extra rotation, and (d) J_4: elbow flexion/extension.

Joint	Actuated DOF	ROM [°]	Nominal Torque [Nm]	Loadcell Range [Nm]	Max Velocity [rad/s]	Transmission type	Transmission ratio	Link Mass [kg]
J_1	S-AA	-50:30	3.48	5.65	2.0	Rigid	26:1	1.75
J_2	S-FE	10:110	20	22.6	2.0	Rigid + AGS	156:1	1.75
J_3	S-HR	0:60	3*3.48	3*5.65	2.0	Cables	(3*26):1	0.75
J_4	E-FE	0:125	10.85	22.6	2.0	Cables	81:1	1.75

TABLE I: Specification of the right-sided AGREE exoskeleton active joints. AGS: Anti-gravity system. ROM: Range-of-motion considering the zero configuration with the arm lying along the trunk. S-AA: shoulder horizontal abdo/adduction, S-FE: shoulder flexion/extension, S-HR: shoulder humeral rotation, E-FE: elbow flexion/extension.

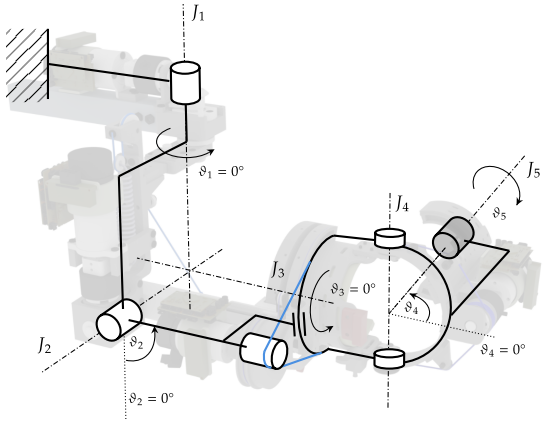


Fig. 2: Kinematic model of the AGREE exoskeleton.

tion/supination movements. A 3D-printed shell is attached to the forearm/wrist and it can rotate about its axis through a curved rail mechanism similar to the J_3 module.

The exoskeleton is provided with re-configurable mechanical end-stops that permit therapists to adjust the range of motion to use the device on the right or left arm. The adjustment does not require the disassembly of parts and the device can be re-configured in few minutes. The total weight of the exoskeleton (excluding the mounting frame and including chassis and cables) is around 8 kg. The detailed masses of the moving links are shown in Tab. I.

B. Actuation and sensors design

Exoskeleton rehabilitation robots are usually provided with electric motors coupled with high transmission ratio gearboxes to increase the generated output torque at each joint, but limiting the mechanical backdrivability of the actuation unit. Each unit is driven by a brushless electric motor (EC45 flat, Maxon Motor AG, Switzerland) coupled with a planetary gearbox (GP-42-C, Maxon Motor AG, Switzerland) of different transmission ration according to the demanded torque requirements. Joint angles are measured by incremental encoders (MILE, Maxon Motor AG, Switzerland), which are referenced to their zero values through an initialization procedure. However, cable-based transmissions introduce elasticity, which is empirically compensated as

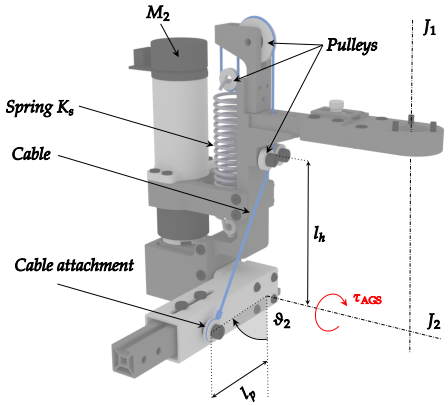


Fig. 3: The AGS mechanical design.

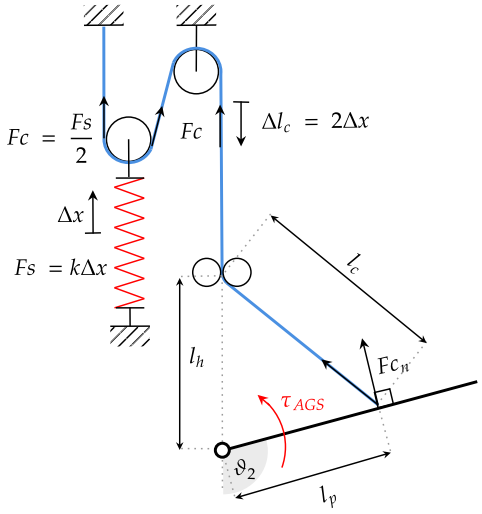


Fig. 4: The AGS static model.

a function of joint torque. Finally, a reaction torsional loadcell (TRT-50/200, Transducer Techniques, CA, USA) is connected to the output shaft of the gearbox to provide a reliable torque signal to measure and reject frictional torques introduced by the transmission. Technical specifications of the actuated joints are listed in Table I. In our work, the compliant behavior is thus obtained independently at each joint. Specifically, we developed a loadcell-based actuation unit and we replicated it for each joint of the exoskeleton.

C. Anti-gravity system (AGS)

The Anti-Gravity System (AGS) is a constant-force mechanism that is used to generate an additional counterweight torque to reduce the gravitational force acting on the motor at the shoulder flexion/extension joint J_2. The rationale behind using an AGS is to reduce the torque requirements of the joint, thus allowing for a more lightweight and efficient actuator. This is particularly important for upper-limb exoskeletons, as they need to be lightweight and easy to wear for extended periods of time. Different techniques have been proposed in the literature for implementing constant-force mechanisms to counterbalance gravity in upper-limb exoskeletons. These include spring-pulley systems [26], [27], variable stiffness lever-based systems [28], and gas spring-based systems [29]. However, only few mechanisms can self-regulate to dynamically adjust the generated torque [30].

In our design, the AGS is intended to generate a variable torque based on the thoracohumeral elevation angle of the joint. The purpose is not to precisely weight-compensate the system across the range-of-motion or adapt the compensation to different arm weights, but rather to reduce the torque requirements of the joint by a fixed amount. To achieve this, we implemented a spring-pulley system, which utilizes an elastic element placed in parallel to the actuation unit. This results in a simpler and more compact design compared to other state-of-the-art solutions.

Fig. 3 shows the proposed mechanism, which consists of a tension spring, a cable, and a set of pulleys. One extremity of the cable is anchored to the link downstream of the J_2 joint at length l_p, and the other extremity is anchored to the previous link through the pulley mechanism shown in Fig. 4. The spring-generated force F_s can be computed as in 1:

$$F_s = K_s(x_s - x_{s0}) \tag{1}$$

where K_s is the spring stiffness, x_s is the spring variable length, while x_{s0} is the spring length at its equilibrium point, i.e., when it does not generate any force. Two additional pulleys have been introduced on the top part of the module to increase the cable elongation, and the operating range of the AGS (Fig. 3). The drawback is that the generated force is reduced, but this issue can be bypassed by increasing the spring stiffness. Consequently, due to the pulleys mechanism, the generated spring force acting on the cable is halved ($F_c = F_s/2$), and the cable elongation is doubled ($\Delta l_c = 2\Delta x$) . Therefore the force acting on the cable F_c becomes:

$$F_c = \frac{1}{2}K_s\frac{1}{2}(l_c - l_{c0}) \tag{2}$$

where l_c and l_{c0} refers to variable and equilibrium cable length respectively, as depicted in Fig. 4. The cable length can be computed as:

$$l_c = \sqrt{l_p^2 + l_h^2 + 2l_p l_h cos\theta_2} \tag{3}$$

where l_p and l_h are shown in Figure 4.

Finally, the AGS counterweight torque τ_{AGS} can be computed as a function of θ_2 as follows:

$$\tau_{AGS} = \frac{1}{4}K_s(l_c - l_{c0})l_p(l_h/l_c)\sin\theta_2 \tag{4}$$

The computed characteristic curve of the developed AGS is represented in Figure 5 with solid red line in the J_2 ROM. The torque plot shows symmetrical behavior with respect to $\theta_2 = 70°$. Indeed, similarly to the RETRAINER exoskeleton [31], the AGS was optimized to generate the maximal restoring torque when the shoulder elevation angle is about 70°, which can be considered the average humeral elevation angle during seated reaching and eating tasks [23].

In this study, we addressed the effects of the AGS by experimentally measuring the AGS-generated torque at the joint J_2 and by comparing it with the theoretical one. The

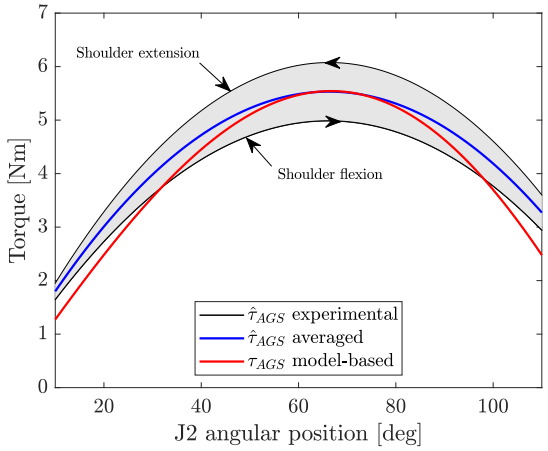


Fig. 5: The AGS counterweight torque (τ_{AGS}). The model-based torque is represented in red. The solid black lines represent the fitted experimental data during respectively flexion (lower line) and extension (upper line) phases. The blue line corresponds to the averaged counterweight torque derived from experiments.

J_2 actuation module was position-controlled spanning the ROM (i.e. 10°-110°, as depicted in Tab. I), and we measured the loadcell-generated torque, which, since no other forces were applied, indicates the AGS-generated torque. Then, we interpolated the experimental data to fit a second-order polynomial equation. Results show that experimental data matches the theoretical model, and that the AGS could provide a maximum torque of approximately 5 Nm at 70°, which is about 25% of the total torque demand. This is a clear indication that thanks to the AGS we could reduce the motor torque requirements of joint J_2.

III. Exoskeleton Control

AGREE has been conceived to operate in different human-robot training modalities according to the residual movement capabilities of the wearer. Indeed, the rehabilitation platform should adapt the arm support and the difficulty of the exercises to maximize the engagement and to challenge the participant during the treatment. To enable the adaptation of the therapy, the AGREE rehabilitation robot implements different training modalities, categorized according to the user's interaction status [5]: passive mode, active assistive mode, and active resistive mode.

As demonstrated in our previous work [19], such training modalities could be intended as a continuum of human-robot interaction, and can be implemented under a unified mid-level control scheme based on impedance control by tuning its parameters as a compromise between good trajectory tracking and transparency to user-initiated movements.

Hence, we developed an impedance-based controller that offers several features, such as favoring good transparency of the joint, compensating for the human arm weight, assisting the motion along a trajectory, or challenging the patient through virtual resistance. With respect to our previous work [19], we replicated the decentralized impedance-based controller for each joint of the exoskeleton, and added a centralized controller for gravity compensation and trajectory generation.

As shown in Figure 6, the control system of the AGREE exoskeleton has been designed with a layered architecture, based on *high-level*, *mid-level* and *low-level* control schemes.

A. Low-level exoskeleton control

The inner control loop is in charge of promoting mechanical compliance and managing the interaction torque between the robot and the user's joints through a loadcell-based torque controller. Hence, robot transparency is achieved by rejecting all friction-based torque disturbances. The feedback torque controller is implemented with a traditional proportional-integrative-derivative (PID) regulator. We empirically tuned the low-level gains at each joint to achieve stable step-response and minimum residual torques during user-generated motion. The torque controller is provided with a feedforward friction compensation term that accounts for both static and viscous friction, as modeled in our previous work, where friction modeling parameters have been identified through proper system identification [19]. Finally, the control signal is fed into a closed-loop motor current controller, embodied in the motor driver.

B. Mid-level exoskeleton control

An impedance controller is implemented through a position-based outer loop as shown in Fig. 6. The commanded joint torque τ_d is computed as the sum of three main contributions:

$$\tau_d = \tau_{fb} + \tau_{ff} + \tau_s \tag{5}$$

where τ_{fb} the feedback impedance-based term, τ_{ff} is the feedforward gravity compensation term, and τ_s is the safety stop term, as shown in Figure 6.

Thus, we introduce a further classification.

1) Feedback impedance-based control: The proposed control scheme relies on the hypothesis that each joint can be independently controlled by a joint-space decentralized control scheme in terms of haptic impedance rendering. Therefore, the controller can be replicated for each joint and it is embedded by a feedback impedance-based controller, which implements a first-order impedance that corrects for trajectory errors through a virtual spring-damper system [17]. From a human-robot interaction perspective, the exoskeleton assists the user in following pre-defined task trajectories by creating a corrective force-field toward the desired angular position. The control law can be expressed in the well-known form:

$$\tau_{fb} = K(\theta_d - \theta_m) - D\dot{\theta}_m \tag{6}$$

where τ_{fb} is the feedback torque for the mid-level controller, K is a virtual stiffness, D is an always positive virtual damping, θ_d and θ_m are respectively the desired reference joint trajectory and the measured joint angle.

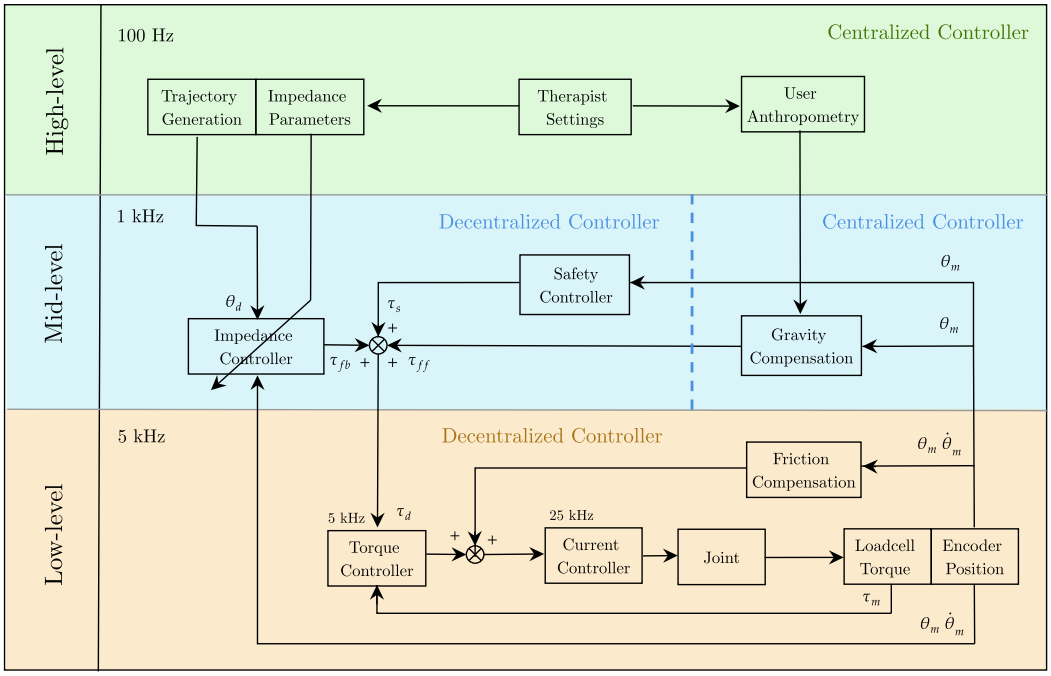


Fig. 6: Architecture of the control system, which is divided in *high-level*, *mid-level* and *low-level*, running at 100 Hz, 1 kHz and 5 kHz, respectively. The *mid-level* is further divided in centralized and decentralized control.

2) Feedforward gravity compensation control: In order to compensate for the gravity of the robot mechanical structure and of the human arm, we implemented a centralized gravity compensation strategy, based on the recursive Newton-Euler inverse dynamics method, which maps motion (and pose) to torque, and iteratively computes the inverse dynamics torques by back-propagating gravitational effects from the end-effector to the base link.

Specifically, for the i^{th} link, we compute the force (f_i) and torque (n_i) acting at the i^{th} frame as:

$$f_i = \mathbf{R}^i_{i+1} f_{i+1} + F_i \tag{7}$$

$$n_i = \mathbf{R}^i_{i+1} n_{i+1} + lc_i \times F_i + l_{i+1} \times \mathbf{R}^i_{i+1} f_{i+1} \tag{8}$$

where F_i is the gravity force applied at the center of mass relative to the i^{th} frame, $\mathbf{R}^i_{i+1} f_{i+1}$ is the rotational transformation from the i^{th} frame to the $i+1^{th}$ frame, lc_i locates the i^th center of mass relative to the i^th frame, and l_{i+1} locates the $i+1^{th}$ frame relative to the i^{th} frame. Finally, the algorithm extracts the $\hat{Z}$ component ($[0\ 0\ 1]^T$) of the resulting torque as follows:

$$\tau_{G_i} = n_i^T \hat{Z} \tag{9}$$

The exoskeleton mechanical properties, including masses and centers of mass, were computed using the detailed CAD model of the system in SolidWorks (Dassault Systèmes). Notably, the centralized gravity compensation method supports both the exoskeleton weight and the human arm weight. The human arm is modeled as two distinct mass points (upper-arm and forearm/hand) applied at the centers of mass of the arm segments. The nominal masses and lengths were obtained from literature anthropometric tables according to user height and weight [21]. To improve the user experience, the weight counterbalance assistance can be tuned by means of a weighting factor to adjust the upper-arm and forearm weight compensation according to the user's feeling. Thus, the gravity force applied at the i^{th} link can be expressed as:

$$F_i = m_{G,i}\hat{\mathbf{g}}_i + W_i m_{H,i}\hat{\mathbf{g}}_i \tag{10}$$

where $\hat{\mathbf{g}}_i$ is the gravity vector relative to the i^{th} frame and W_i are the weighting factors, $m_{G,i}$ denote the robot masses, $m_{H,i}$ are the human segments masses:

$$m_{H,i} = \begin{cases} 0 & \text{if } i = 1,3 \\ m_{ua} & \text{if } i = 2 \\ m_{fa} & \text{if } i = 4 \end{cases} \tag{11}$$

The effect of the AGS is included in this calculation by subtracting the AGS-generated torque τ_{AGS} from the computed τ_{G_2} gravitational torque. In this way, the controller is aware that the spring element compensates for part of the weight of the robot. Finally, the computed torques are positively fed to the joint-space impedance controllers as feedforward contributions (τ_{ff}), see Fig. 6.

3) Safety stop control: To guarantee safety during operation, the AGREE control system is embedded with safety measures that limit joint torques, angular position, or velocities at their maximum values (Table I). In addition, software end-stops are introduced to smoothly restrict the ROM during robot operation, by progressively counteracting the motion as the user moves the arm to the limits of the ROM. The software end-stops are implemented with a repulsive

impedance controller at the boundaries of the ROM (θ_{min}, θ_{max}), through a virtual spring-damper system, namely K_s and D_s, as described in eq. (12). The end-stops are enabled only within a certain tolerance (θ_{tol}) from the ROM limit. In our case $\theta_{tol} = 5°$.

$$\tau_{s,i} = \begin{cases} -K_s(\theta_{max} - \theta_i) - D_s\dot{\theta}_i & \text{if } \theta_i > \theta_{max} - \theta_{tol} \\ -K_s(\theta_{min} - \theta_i) - D_s\dot{\theta}_i & \text{if } \theta_i < \theta_{min} + \theta_{tol} \\ 0 & \text{otherwise} \end{cases} \tag{12}$$

C. High-level exoskeleton control

The *high-level* control is responsible for three main features.

Firstly, a trajectory generator computes reference joint trajectories for the desired task. In detail, with the AGREE system, exercises are usually performed on a table placed in front of the patient, and the desired hand movement is computed by interpolating via-points that are selectable through a graphical interface [20]. An inverse kinematics algorithm computes the joint-space configuration for each via-point based on the desired hand position. Hand orientation is not included in the algorithm since it can be independently modified by the wrist prono/supination passive joint. Thus, the kinematic redundancy of the arm is exploited to avoid singularities and account for joint limits. Finally, in order to guarantee minimum jerk trajectories, a fifth-order interpolator is used to build the final joint profiles.

Secondly, the AGREE system was built to offer the possibility to widely customize the training exercises. Precisely, the operating mode, weight compensation assistance and movement speed can be adjusted through a graphical user interface. In particular, as previously presented in [19], a proper combination of stiffness and damping is employed to render different human-robot interaction modalities. For instance, *passive-assisted mode* can be achieved with high stiffness and low damping, while *active-resistive mode* is characterized by low stiffness and high damping, as described in the following Section IV.

Lastly, the high-level controller is also aimed at managing the operational workflow of the rehabilitation platform. To avoid abrupt changes in torques and forces applied to the human arm, a smoothing function is used to harmonize variations every time the exoskeleton changes its operating mode. At each state transition, the smoothing function is applied to desired feedforward torque, position, stiffness, and damping values, as follows:

$$y(t, y_i, y_f) = y_i + \frac{(y_f - y_i)}{2}\left(\tanh\left(\frac{t}{T} - \exp\right) + 1\right) \tag{13}$$

where t represents time, y_i and y_f are respectively the initial and final values, and T is the time constant, which we fixed to 1 second for smooth transitions.

D. Control hardware

The AGREE exoskeleton is operated by a Linux-based real-time control unit. The unit is equipped with a real-time C++ library, based on the Simple Open-Source EtherCAT Master (SOEM), to handle the communication with motors and sensors. The *high-level* exoskeleton control, which is responsible for trajectory generation and impedance-based control parameters setting, is operated through the Robotic Operating System (ROS) and runs in *soft* real-time at 100 Hz. The *mid-level* impedance-based controllers and the gravity compensation algorithm run in *hard* real-time at 1 kHz. Finally, the *low-level* control loop runs at 5 kHz and is implemented within the motor drivers (Mini Torque Driver, Harmonic Bionics, Austin, TX). The loadcell-based torque signals are conditioned and amplified by the motor driver, and filtered and down-sampled to 1 kHz to avoid aliasing errors.

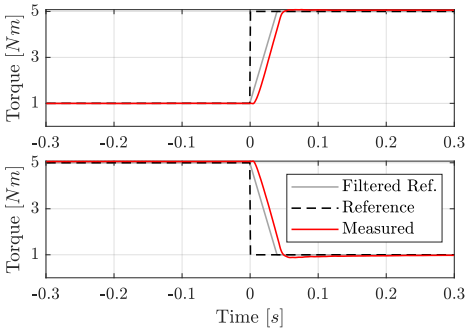


Fig. 7: Torque step response for increasing and decreasing steps on the J4 actuation unit locked at its end-stop.

Direction	**Rising Time** [s]	**Settling Time** [s]	**Settling Error** [Nm]	**Overshoot Torque** [m]
Increasing	0.03 ± 0.00	0.07 ± 0.04	0.06 ± 0.14	0.11 ± 0.18
Decreasing	0.03 ± 0.00	0.10 ± 0.06	0.01 ± 0.11	0.14 ± 0.23

TABLE II: Torque step response results.

IV. CONTROL CHARACTERIZATION RESULTS

We conducted several experimental trials to characterize the control system performances and validate the capability to promote different human-robot interaction modalities. Experiments were conducted to assess the performance of the control system at *low-level* and *mid-level*. All the experiments that involved human subjects were approved by the Ethical Committee of Politecnico di Milano (Opinion n. 13/2021).

A. Low-level control validation (Torque controller)

We assessed the performance of the *low-level* torque controller on the elbow flexion/extension actuation unit, which we considered a representative joint for the AGREE exoskeleton. Indeed, the J4 unit, which actuates the elbow flexion/extension, has the typical architecture of the other joints, and it can generate up to 15 Nm. Furthermore, it is actuated through a cable-based transmission which introduces additional elasticity and backlash.

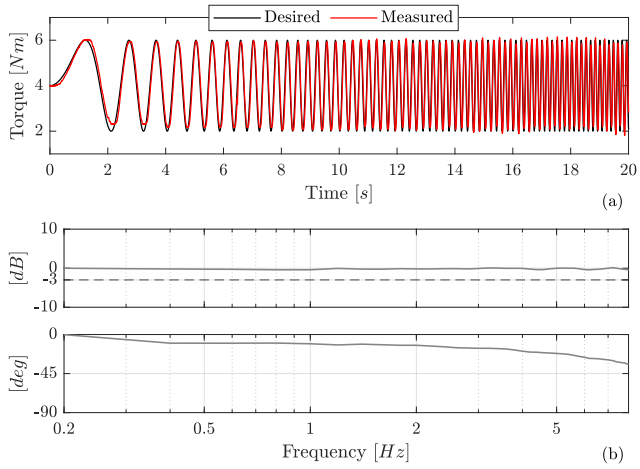


Fig. 8: Torque chirp response. (a) Snapshot of the torque tracking response of the chirp reference signal ranging from 0.5 Hz to 8 Hz over about 150s. (b) Bode diagram of amplitude and phase of the torque closed loop bandwidth.

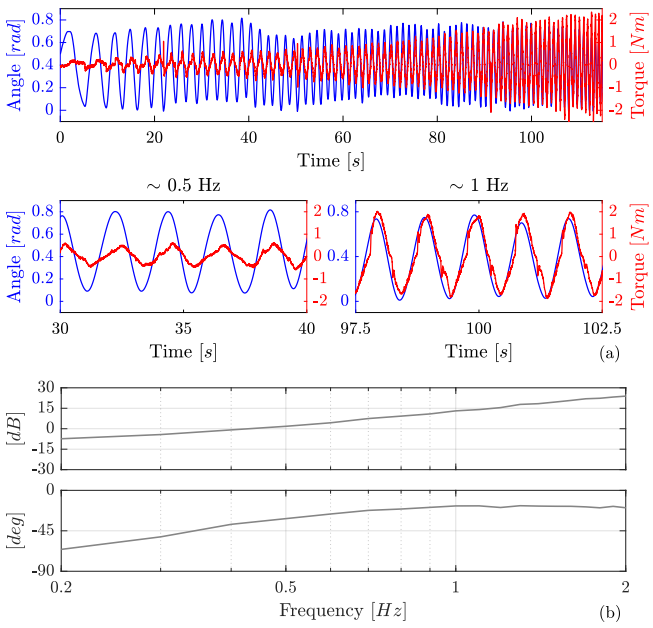


Fig. 9: Joint transparency impedance. (a) Raw data of the elbow/flexion extension transparency test at different frequencies. (b) Bode diagrams of amplitude and phase of the residual joint transparency impedance.

1) Step response: We evaluated the step response for increasing and decreasing torque steps of 4 Nm over 25 repetitions. The experiments were performed in static conditions, i.e., with $\dot{\theta}_i = 0$. Fig. 7 shows the step response results. The desired step (dotted black line) is filtered (gray line) not to operate torque changes greater than 0.1 Nm/ms. As shown in Tab. II, results proved stable behavior with fast response, with settling time below 0.1 seconds for 4 Nm torque steps.

2) Frequency response: The frequency response was evaluated through a chirp signal with a sinusoidal peak-to-peak amplitude of 4 Nm and with frequency linearly increasing from 0.2 Hz to 8 Hz over about 150 s. We computed the system transfer function estimate with an H1 frequency estimator. We repeated the chirp response three times and computed magnitude and phase Bode plots. Fig. 8(a) shows the chirp response in the time domain, demonstrating that the torque controller could track with high accuracy the commanded signals. Fig. 8(b) shows that the torque control magnitude was always enclosed in the $\pm$3dB band and a maximum phase lag of 35°, demonstrating suitable performance in the human frequency range.

3) Joint transparency impedance: A healthy participant performed elbow flexion/extension sinusoidal movements with the joint in transparent mode. The user followed a visual feedback commanding peak-to-peak amplitude of 45° and frequencies from 0.2 Hz to 2 Hz. Results are shown in Fig. 9(a). Maximum peak torques at 0.5 Hz (corresponding to 1 rad/s) and 1 Hz (corresponding to the maximum velocity of 2 rad/s) are 0.5 and 2 Nm, respectively. Furthermore, we computed the joint transparency impedance as the ratio between the measured torque and the angle value (i.e., the residual stiffness perceived by the user) and we calculated the frequency response, shown in Fig. 9(b). Results show that the amplitude of the frequency response at 0.5 Hz resulted in about +2 dB, corresponding to a residual stiffness of 1.25 Nm/rad, while at 2 Hz the frequency response was +24 dB, corresponding to a maximum residual stiffness of about 15 Nm/rad. Furthermore, the Bode plot shows greater phase lag at low frequencies, probably due to friction-induced disturbances.

B. Mid-level control validation (Impedance controller)

Regarding the *mid-level* controller, the control system performance has been presented in our previous work and tested with a single-joint orthosis [19]. In this work, we conducted further experimental trials both with and without a human subject with a multi degrees-of-freedom system.

1) Single-joint impedance exploration: To assess the impedance controller and the baseline joint tracking error, we performed single-joint trajectories while sampling stiffness K and damping D parameters (i.e., the K-D space), and we evaluated the baseline tracking error. We employed sinusoidal trajectories exploring the range of motion of each joint. All trajectories - apart from the trajectory executed by the J2 joint, which necessarily moves against gravity - are performed in zero-gravity planes, to minimize the gravitational effect. While the desired joint is tested, *ceteris paribus*, all the others are fixed at a nominal position. Maximum stiffness/damping values were derived from nominal torque specifications.

For each combination of stiffness and damping, we recorded the desired and measured angular positions, and we computed the trajectory Root Mean Squared Error (RMSE) over five sinusoidal repetitions.

To evaluate the accuracy of the weight compensation algorithm, we repeated the experiments with and without the subject. In all experiments, the subject was asked to

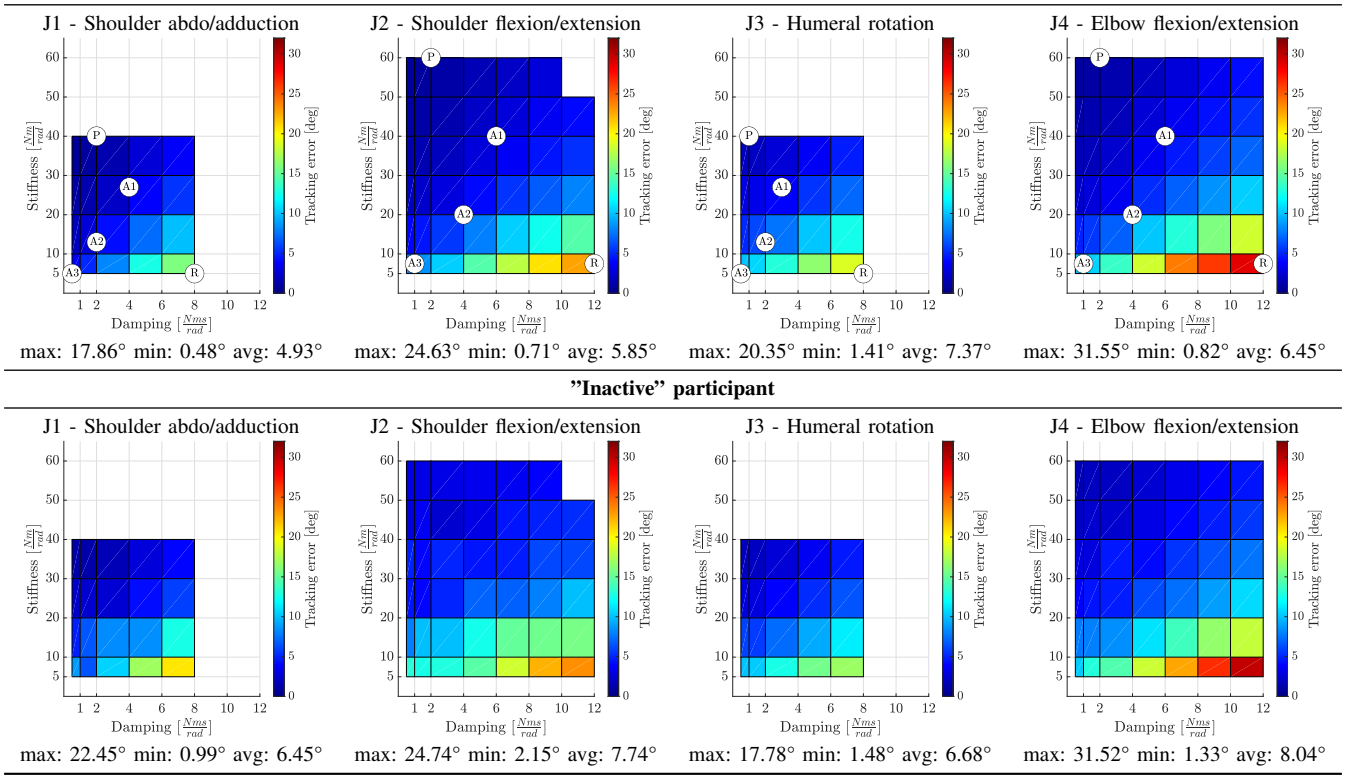
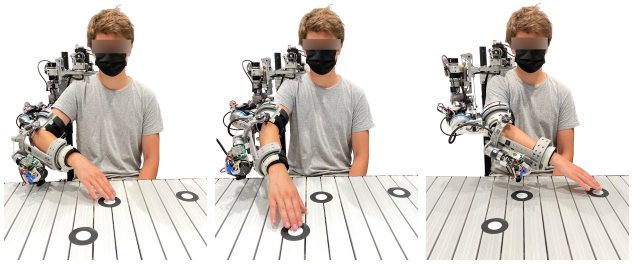


TABLE III: K-B plots displaying error in tracking movement of different joints in the single-joint impedance test. First row with no participant, second row with "inactive" participant. White circles indicate the selected stiffness and damping for the five modalities used during multi-joint reaching tasks. P: *passive-assisted*, A1-A2-A3: *active-assisted*, R: *active-resistive*.

behave "passively" to exclude any voluntary effort from the characterization. The experiments aim to understand the joint behavior as stiffness and damping change, and we strove to demonstrate whether all joints can achieve comparable results. Tab. III shows the trajectory tracking RMSE results for each joint, with an "inactive" participant wearing the exoskeleton and without the participant. We can notice that minimum tracking errors occur with high stiffness and low damping values, while maximum errors are present with high damping values. Notably, with these results we demonstrate that different K-D parameters can increase and decrease the baseline tracking error.

2) Multi-joint reaching task: we tested the exoskeleton with a multi-joint reaching task by sampling the K-D space according to the desired haptic feedback. In detail, we selected five modalities that require different human effort to fulfill the movement successfully.

The impedance parameters are shown with white circles in Tab. III (i.e., P, A1, A2, A3, and R). For instance, for the *passive-assisted* mode (P), we selected high stiffness and low damping values to improve trajectory tracking and rigidly guide the user. Instead, if more compliant interaction is desired, K can be decreased to introduce larger baseline tracking errors. Hence, with *active-assisted* modalities (A1, A2, A3), the movement is supported across the task, but the user can deviate from the nominal trajectory. Finally,



(a) Point P_0 (b) Point P_1 (c) Point P_2

Fig. 10: The multi-joint three-points reaching task. The exercise sequence is: $P_0 \rightarrow P_1 \rightarrow P_0 \rightarrow P_2 \rightarrow P_0$.

to implement an *active-resistive* mode (R), by which the robot resists the user's motion, high damping values can increase the baseline tracking error through viscous-like forces. Overall, we increased the stiffness to enhance the corrective assistance, while we increased the damping to reduce overshoots and oscillations and to introduce a baseline tracking error, which should engage the user to follow the desired trajectory.

Regarding the desired movement, we performed a reaching exercise on the horizontal plane in front of the exoskeleton. We selected three representative end-points in the reachable workspace (one in front of the user, one on the left, and one in the front-right direction), shown in Fig. 10, to be

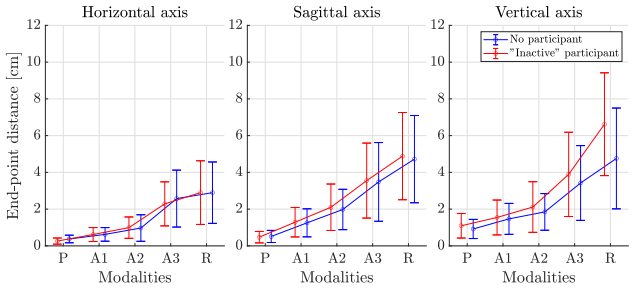


Fig. 11: End-point distance during reaching tasks, evaluated for each modality with and without the participant. P: *passive-assisted*, A1-A2-A3: *active-assisted*, R: *active-resistive*.

reached by the exoskeleton end-effector (i.e., the participant's hand). We generated the exercise trajectories through the IK algorithm imposing a maximum peak velocity of 2 rad/s.

We performed ten repetitions of the reaching task under two conditions, i.e., when there is no participant involved, and when a participant is wearing the exoskeleton, but not actively participating in the task. We repeated the procedure for each selected modality. End-point reaching errors, shown in Fig. 11, were computed from the arm kinematic model as the distance between the target end-point and the exoskeleton end-effector positions, and averaged across different end-points and repetitions. Fig. 11 shows the end-point reaching distance during the reaching tasks across five modalities, and its parameters are represented in Tab. III.

Results show increasing end-point reaching errors as the assistance decreases. As expected, the *passive-assisted* mode achieved good reaching accuracy, with an averaged end-point error of 1.2 cm and 1.1 cm, respectively with and without the participant. Instead, maximum end-point reaching errors were obtained in *active-resistive* mode, with errors of 8.7 cm and 7.3 cm. These results demonstrate that the observed behavior on the single joint is replicated at the end-effector level.

The optimization of K and D parameters is not the scope of this work. We support the idea that such parameters can be exploited as a continuum of rehabilitation modalities, and we believe such parameters can be tuned according to the stage of motor recovery towards the personalization of the treatment.

V. Discussion

This work introduced the mechatronic and control design of the AGREE exoskeleton, and we conducted preliminary experiments to specifically demonstrate the feasibility of the control approach.

A. Mechatronic design

The major contribution of the mechatronic design regards the employment of reaction torque sensors at each joint of the exoskeleton as compared to multi-axis force/torque sensors [18], [32] or SEA-based approaches [10], [16]. Specifically, we employed high-stiffness torsional loadcells connected to the gearbox output shafts. The employment of loadcell-based actuation units permitted to achieve stable behavior (wider torque control bandwidth) with higher virtual stiffness as compared to SEAs [17], [10] and to promote good transparent behavior against both user-generated and externally-applied forces, which is not possible with force/torque sensors attached at the interface points [18], [13].

The kinematic chain of the AGREE exoskeleton has been designed to support movements of the shoulder and elbow. Considering the shoulder, in the literature, several robotic exoskeletons offer complex mechanisms to address residual movements of the shoulder girdle and promote the scapulo-humeral rhythm [24], [10], [33]. In our work, to reduce encumbrance, weight, complexity, and costs, the AGREE exoskeleton was designed to only support the main movements of the shoulder complex that we approximate with a ball-socket joint [11]. Also, similarly to the ARMin exoskeleton [18], the mechanical design is symmetric to favor use with both right and left arms. Indeed, post-stroke rehabilitation usually involves one arm at a time, and this feature allows the use of the proposed rehabilitation exoskeleton with both right-side and left-side impaired patients.

With AGREE, we developed a lightweight robotic exoskeleton embodied with an AGS counterbalance mechanism, which allowed, considering slow movements and low inertia torques, to reduce the motor torque requirements. Indeed, the total weight of the moving arm (around 6 kg) is lower than other rehabilitation exoskeletons provided with a similar number of active DOFs, such as ARMin III-V (around 19 kg) [18], NESM-γ (12.8 kg) [16] or ANYexo (13 kg) [9]. Thanks to the novel design of the AGS and the lightweight exoskeletal structure, we could reduce the nominal torque requirements at the joints. In detail, to compensate for the arm weight of the 95^{th} percentile user, our actuation units can support up to 15.0 Nm and 20.0 Nm respectively for elbow flexion/extension and shoulder elevation, compared to 32.0 Nm and 37.8 Nm of the ARMin III exoskeleton [18], to 30.0 Nm and 60.0 Nm of the NESM exoskeletons [10], [16] to 13.0 Nm and 34.4 Nm of the Harmony exoskeleton [8], or to 9.0 Nm and 28.0 Nm of the RECUPERA exoskeleton [32]. Although our exoskeleton has significantly smaller torque requirements, our results demonstrated that the assistive torques generated by the system (excluding the gravity compensation for exoskeleton links) are suitable to compensate for the arm weight and to support trajectory-based movements.

B. Control characterization

We implemented a unified compliant control framework based on explicit impedance control, and we ran some trials to evaluate the controller performances. Firstly, we implemented an explicit closed-loop torque controller for each joint, which rejects residual disturbances thanks to the loadcell-based torque feedback. We analyzed the frequency response with a chirp signal up to 8 Hz and the torque-controlled joint transfer function resulted in the $\pm$3dB bandwidth for all frequencies. Since arm voluntary movement

bandwidth is usually limited to 2 Hz [22], we did not investigate higher frequency response. Other exoskeletons achieved similar results: the NESM exoskeleton presents a torque control bandwidth of 6.9 Hz the 10 Hz [10], the NESM-γ has bandwidth up to 10 Hz [16], while the Harmony exoskeleton is torque-controlled up to 7 Hz [8]. However, employing direct torque-feedback through an explicit torque control loop requires non-trivial parameters tuning as a trade-off between low undesired residual torques and a bigger range of achievable stiffness. In fact, when dealing with explicit impedance control, such as in our application, the inner torque closed-loop can strongly influence the bandwidth of achievable impedance ranges. As presented by Focchi and colleagues [34], achieving high control bandwidth for the torque control loop might not be beneficial if a wide range of rendered stiffness is desired.

Furthermore, we demonstrated joint transparency by performing user-generated backdriving movements when the joint is controlled in transparent mode. Results show peak residual torques of 0.5 Nm with joint velocities around 1.0 rad/s. In [13], the ARMin IV+ exoskeleton obtained peak torques around 2.0 Nm. Similarly, Kim and colleagues [8] achieved backdrivability with residual torques $<$ 0.3 Nm for joint velocities $<$ 0.6 rad/s. Additionally, we computed the joint transparency impedance as the transfer function between measured residual torques and joint angle. Results show maximum residual stiffness at 2 Hz of about 15 Nm/rad, which is comparable with the NESM exoskeleton [10].

With these results, we posit that the torque controller could reject most frictional disturbances, and that minimal resistive torques are perceived when the user explores the workspace in free-motion. We underline the importance of achieving transparency, measured as the ability of the exoskeleton of not applying resistive/assistive forces to free motion [6]. Indeed, the exoskeleton should not resist but guide the subject's voluntary activity during the exercise.

Secondly, we implemented an active gravity compensation method to support the weight of the human-robot system. Indeed, achieving a good gravity compensation model is preeminent for improving transparency when the user drives the robot during active workspace exploration. However, since rehabilitation exercises are usually performed at low-speeds and following minimum-jerk trajectories [18], we simplified the dynamic model to a quasi-static model and the dynamic terms due to velocity and inertia were neglected.

Finally, to validate the performance of the control system in a real-world scenario, we performed some preliminary experiments on one healthy participant. The primary objective of the experimental characterization was to demonstrate the feasibility of the control approach, but we suggest that further testing on a larger and diverse population is necessary to fully validate the control approach. While the output impedance has been validated in a previous work on a single-joint orthosis [19], here, we assessed the residual tracking performance when the exoskeleton is commanded to follow sinusoidal single-joint and multi-joint trajectories. Results show that the controller can follow reference trajectories and potentially engage the users by inducing them to correct the movement through a wide range of haptic feedback. These tests allowed us to assess the exoskeleton performance in terms of its ability to follow the desired trajectory, and its compliance to human-generated forces.

C. Neurorehabilitation perspectives

Common upper-limb rehabilitation platforms can perform mobilization exercises in various training modalities, such as passive, active assistive, assisted-as-needed, or resistive modalities. State-of-the-art robotic exoskeletons, such as Harmony [8], NESM [10] or ARMin [18], can operate in different rehabilitation training modalities that the therapists can select during the rehabilitation session. Similarly, we demonstrated that the AGREE exoskeleton can generate assistive or resistive force-fields depending on the desired physical human-robot interaction.

Our study confirms that different combinations of stiffness and damping values in the exoskeleton can lead to a wide range of haptic impedance, which can be used to deliver various rehabilitation modalities, from passive mobilization to resistive training. This is in line with the findings of [19], where it is shown that different training modalities can be identified by sampling the K-D space. Our experimental trials during reaching tasks showed that high stiffness values generate more accurate trajectory tracking, while high damping values introduce resistive forces leading to greater baseline end-point distance errors. The end-point distance can in turn be considered an indicator of the available range for human volitional contribution. Therefore, small discrepancies are expected in the *passive-assisted* mode, where user contribution is supposed to be minimal. On the other hand, in the *active-assisted* and *active-resistive* modalities, we aim to achieve larger discrepancies, where the participant is expected to contribute with increasing effort. Our study provides a foundation for future research in the field of upper-limb exoskeletons. However, further testing on the target population is needed to fully understand the effects of our device on the physiological motor control strategies of post-stroke survivors. In the future, we plan to validate the exoskeleton by measuring interaction forces and human voluntary activity through electromyography, building on the previous work we performed on a single degree-of-freedom [19]. This will give a better understanding of the exoskeleton performance and effects on human physiology.

VI. CONCLUSION

In this work, we presented the mechanical and control design of the AGREE exoskeleton, an upper-limb robotic device for post-stroke rehabilitation. The main novelty of the exoskeleton regards the employment of loadcell-based actuation units and the implementation of a unified control architecture that allows the exoskeleton to behave compliantly to forces generated by the users and the therapists. Indeed, thanks to the torque-controlled actuation units, the exoskeleton allows direct physical interaction with therapists

and real objects, allowing the development of novel control strategies for functional rehabilitation. With the experimental validation results, we verified that the robotic system could behave transparently to user volitional movements, as well as support the arm during trajectory-based tasks, with different levels of assistance. Finally, we demonstrated that the robotic system could potentially engage the patients by inducing them to correct a broad range of tracking errors, which confirms the potential suitability of the AGREE exoskeleton for the neurorehabilitation treatment. This exoskeleton could serve as a research platform for future rehabilitation treatment, based on adaptability and customization of exercises.

REFERENCES

[1] A. Cieza, K. Causey, K. Kamenov, S. W. Hanson, S. Chatterji, and T. Vos, "Global estimates of the need for rehabilitation based on the Global Burden of Disease study 2019: a systematic analysis for the Global Burden of Disease Study 2019," *The Lancet*, vol. 396, pp. 2006–2017, 12 2020.

[2] W. Johnson, O. Onuma, M. Owolabi, and S. Sachdev, "Stroke: a global response is needed," *Bulletin of the World Health Organization*, vol. 94, pp. 634–634, 9 2016.

[3] G. Fattore, A. Torbica, A. Susi, A. Giovanni, G. Benelli, M. Gozzo, and V. Toso, "The social and economic burden of stroke survivors in Italy: a prospective, incidence-based, multi-centre cost of illness study," *BMC Neurology 2012 12:1*, vol. 12, pp. 1–11, 11 2012.

[4] W. H. Chang and Y.-H. Kim, "Robot-assisted Therapy in Stroke Rehabilitation," *Journal of Stroke*, vol. 15, no. 3, p. 174, 2013.

[5] A. Basteris, S. M. Nijenhuis, A. H. Stienen, J. H. Buurke, G. B. Prange, and F. Amirabdollahian, "Training modalities in robot-mediated upper limb rehabilitation in stroke: A framework for classification based on a systematic review," *Journal of NeuroEngineering and Rehabilitation*, vol. 11, pp. 1–15, 7 2014.

[6] T. Proietti, V. Crocher, A. Roby-Brami, and N. Jarrasse, "Upper-limb robotic exoskeletons for neurorehabilitation: A review on control strategies," *IEEE Reviews in Biomedical Engineering*, vol. 9, pp. 4–14, 2016.

[7] M. A. Gull, S. Bai, and T. Bak, "A review on design of upper limb exoskeletons," *Robotics*, vol. 9, no. 1, pp. 1–35, 2020.

[8] B. Kim and A. D. Deshpande, "An upper-body rehabilitation exoskeleton Harmony with an anatomical shoulder mechanism: Design, modeling, control, and performance evaluation," *International Journal of Robotics Research*, vol. 36, pp. 414–435, 4 2017.

[9] Y. Zimmermann, A. Forino, R. Riener, and M. Hutter, "ANYexo: A Versatile and Dynamic Upper-Limb Rehabilitation Robot," *IEEE Robotics and Automation Letters*, vol. 4, pp. 3649–3656, 10 2019.

[10] E. Trigili, S. Crea, M. Moisè, A. Baldoni, M. Cempini, G. Ercolini, D. Marconi, F. Posteraro, M. C. Carrozza, and N. Vitiello, "Design and experimental characterization of a shoulder-elbow exoskeleton with compliant joints for post-stroke rehabilitation," *IEEE/ASME Transactions on Mechatronics*, vol. 24, pp. 1485–1496, 8 2020.

[11] J. C. Perry, J. Rosen, and S. Burns, "Upper-limb powered exoskeleton design," *IEEE/ASME Transactions on Mechatronics*, vol. 12, no. 4, pp. 408–417, 2007.

[12] S. Dalla Gasperina, L. Roveda, A. Pedrocchi, F. Braghin, and M. Gandolla, "Review on Patient-Cooperative Control Strategies for Upper-Limb Rehabilitation Exoskeletons," *Frontiers in Robotics and AI*, vol. 8, pp. 1–24, 12 2021.

[13] F. Just, O. Ozen, P. Bosch, H. Bobrovsky, V. Klamroth-Marganska, R. Riener, and G. Rauter, "Exoskeleton transparency: feed-forward compensation vs. disturbance observer," *at - Automatisierungstechnik*, vol. 66, pp. 1014–1026, 12 2018.

[14] Y. Shen, J. Sun, J. Ma, and J. Rosen, "Admittance Control Scheme Comparison of EXO-UL8: A Dual-Arm Exoskeleton Robotic System," in *2019 IEEE 16th International Conference on Rehabilitation Robotics (ICORR)*, vol. 2019-June, pp. 611–617, IEEE, 6 2019.

[15] A. Zeiaee, R. S. Zarrin, A. Eib, R. Langari, and R. Tafreshi, "CLEVERarm: A Lightweight and Compact Exoskeleton for Upper-Limb Rehabilitation," *IEEE Robotics and Automation Letters*, vol. 7, no. 2, pp. 1880–1887, 2022.

[16] J. Pan, D. Astarita, A. Baldoni, F. Dell'Agnello, S. Crea, N. Vitiello, and E. Trigili, "NESM-γ : An Upper-Limb Exoskeleton With Compliant Actuators for Clinical Deployment," *IEEE Robotics and Automation Letters*, vol. 7, pp. 7708–7715, 7 2022.

[17] A. Calanca, R. Muradore, and P. Fiorini, "A review of algorithms for compliant control of stiff and fixed-compliance robots," *IEEE/ASME Transactions on Mechatronics*, vol. 21, pp. 613–624, 4 2016.

[18] T. Nef, M. Guidali, and R. Riener, "ARMin III – arm therapy exoskeleton with an ergonomic shoulder actuation," *Applied Bionics and Biomechanics*, vol. 6, pp. 127–142, 7 2009.

[19] S. Dalla Gasperina, V. Longatelli, F. Braghin, A. Pedrocchi, and M. Gandolla, "Development and Electromyographic Validation of a Compliant Human-Robot Interaction Controller for Cooperative and Personalized Neurorehabilitation," *Frontiers in Neurorobotics*, vol. 15, p. 165, 1 2022.

[20] S. Dalla Gasperina, V. Longatelli, M. Panzenbeck, B. Luciani, A. Morosini, A. Piantoni, P. Tropea, F. Braghin, A. Pedrocchi, and M. Gandolla, "AGREE: an upper-limb robotic platform for personalized rehabilitation, concept and clinical study design*," in *IEEE International Conference on Rehabilitation Robotics, ICORR*, 2022.

[21] D. A. Winter, *Biomechanics and Motor Control of Human Movement: Fourth Edition*, vol. 7. John Wiley & Sons, Inc., 2009.

[22] J. Rosen, J. C. Perry, N. Manning, S. Burns, and B. Hannaford, "The human arm kinematics and dynamics during daily activities - Toward a 7 DOF upper limb powered exoskeleton," *2005 International Conference on Advanced Robotics, ICAR '05, Proceedings*, vol. 2005, pp. 532–539, 2005.

[23] D. J. Magermans, E. K. Chadwick, H. E. Veeger, and F. C. Van Der Helm, "Requirements for upper extremity motions during activities of daily living," *Clinical Biomechanics*, vol. 20, pp. 591–599, 7 2005.

[24] B. Kim and A. D. Deshpande, "Controls for the shoulder mechanism of an upper-body exoskeleton for promoting scapulohumeral rhythm," *IEEE International Conference on Rehabilitation Robotics*, vol. 2015-Septe, pp. 538–542, 2015.

[25] D. P. Romilly, C. Anglin, R. G. Gosine, C. Hershler, and S. U. Raschke, "A Functional Task Analysis and Motion Simulation for the Development of a Powered Upper-Limb Orthosis," *IEEE Transactions on Rehabilitation Engineering*, vol. 2, no. 3, pp. 119–129, 1994.

[26] Q. Wu, X. Wang, and F. Du, "Development and analysis of a gravity-balanced exoskeleton for active rehabilitation training of upper limb," *Proceedings of the Institution of Mechanical Engineers, Part C: Journal of Mechanical Engineering Science*, vol. 230, pp. 3777–3790, 12 2016.

[27] P. W. Hill, E. T. Wolbrecht, and J. C. Perry, "Gravity compensation of an exoskeleton joint using constant-force springs," *IEEE International Conference on Rehabilitation Robotics*, vol. 2019-June, pp. 311–316, 6 2019.

[28] Z. Li, Y. Liu, C. Chen, G. Yang, and S. Bai, "Modeling and design of a reconfigurable novel constant-force mechanism for assistive exoskeletons," *Proceedings of the Institution of Mechanical Engineers, Part C: Journal of Mechanical Engineering Science*, vol. 236, pp. 9941–9950, 9 2022.

[29] J. Hull, R. Turner, A. A. Simon, and A. T. Asbeck, "A Novel Method and Exoskeletons for Whole-Arm Gravity Compensation," *IEEE Access*, vol. 8, pp. 143144–143159, 2020.

[30] D. X. Chew, K. L. Wood, and U. X. Tan, "Design of a passive self-regulating gravity compensator for variable payloads," *Journal of Mechanical Design, Transactions of the ASME*, vol. 141, 10 2019.

[31] E. Ambrosini, J. Zajc, S. Ferrante, G. Ferrigno, S. Dalla Gasperina, M. Bulgheroni, W. Baccinelli, T. Schauer, C. Wiesener, M. Russold, M. Gfoehler, M. Puchinger, M. Weber, S. Becker, K. Krakow, N. Immick, A. Augsten, M. Rossini, D. Proserpio, G. Gasperini, F. Molteni, and A. Pedrocchi, "A Hybrid Robotic System for Arm Training of Stroke Survivors: Concept and First Evaluation," *IEEE Transactions on Biomedical Engineering*, vol. 66, pp. 3290–3300, 12 2019.

[32] S. Kumar, H. Wöhrle, M. Trampler, M. Simnofske, H. Peters, M. Mallwitz, E. Kirchner, and F. Kirchner, "Modular Design and Decentralized Control of the Recupera Exoskeleton for Stroke Rehabilitation," *Applied Sciences*, vol. 9, p. 626, 2 2019.

[33] Y. Zimmermann, E. B. Kucuktabak, F. Farshidian, R. Riener, and M. Hutter, "Towards dynamic transparency: Robust interaction force tracking using multi-sensory control on an arm exoskeleton," in *IEEE International Conference on Intelligent Robots and Systems*, pp. 7417–7424, Institute of Electrical and Electronics Engineers Inc., 10 2020.

[34] M. Focchi, G. A. Medrano-Cerda, T. Boaventura, M. Frigerio, C. Semini, J. Buchli, and D. G. Caldwell, "Robot impedance control and passivity analysis with inner torque and velocity feedback loops," *Control Theory and Technology*, vol. 14, no. 2, pp. 97–112, 2016.